

Noninvasive Temperature Estimation Based on Texture Features of Ultrasound Images for RFA

Ming Chen

Southeast University <https://orcid.org/0000-0002-7931-0356>

Xingqun Zhao

Southeast University

Linfang Yao (✉ yaolinfang47@163.com)

Nanjing Drum Tower Hospital: Nanjing University Medical School Affiliated Nanjing Drum Tower Hospital

Research

Keywords: Ultrasound, Noninvasive temperature estimation, Radio frequency ablation, Wavelet transform, Gray-level gradient co-occurrence matrix

Posted Date: January 7th, 2021

DOI: <https://doi.org/10.21203/rs.3.rs-139349/v1>

License: © ⓘ This work is licensed under a Creative Commons Attribution 4.0 International License.

[Read Full License](#)

1 **Noninvasive Temperature Estimation Based on Texture Features** 2 **of Ultrasound Images for RFA**

3 Ming Chen¹, Xingqun Zhao^{1*}, Linfang Yao^{2*}

4 **Abstract**

5 **Background:** Hyperthermia is one of the most common therapy for tumor, in which
6 temperature monitoring is essential. Invasive temperature monitoring is mostly used
7 in clinic at present, which leads to limited points under monitoring and extra hurt to
8 patients. Therefore, noninvasive temperature estimation is a key and tough problem in
9 hyperthermia. In this paper, a noninvasive temperature estimation method for
10 hyperthermia based on B-mode ultrasonic image with wavelet transform and texture
11 analysis is proposed.

12 **Methods:** Animal tissue both in vitro and in vivo(pig kidneys in vitro and rabbit
13 kidney in vivo) were taken as experimental materials. Ultrasound images and
14 temperature data were collected from radio frequency ablation experiment under
15 approved protocol. Image subtraction and wavelet transform were performed on the
16 ultrasound images to enhance the change during ablation, after which texture features
17 were extracted to analyze the relationship with temperature.

18 **Results:** Texture features hybrid entropy and energy extracted from gray-level
19 gradient co-occurrence matrix of ultrasound images processed had higher linear
20 correlation with temperature than traditional gray value method. From in vitro and in
21 vivo experiments, the linear correlation coefficients obtained between hybrid entropy

Corresponding authors: ¹Xingqun Zhao Email address: ndt@seu.edu.cn

² Linfang Yao Email address: yaolinfang47@163.com

22 and temperature were 0.979 ± 0.028 and -0.935 ± 0.037 , respectively, and those between
23 energy and temperature were 0.932 ± 0.056 and -0.915 ± 0.034 , respectively. In addition,
24 the slopes of linear model obtained in vitro were relatively consistent, while those
25 under in vivo condition had certain individual differences.

26 **Conclusions:** The results demonstrated that texture features hybrid entropy and
27 energy of ultrasound image processed with the method proposed in this paper can be
28 used for temperature estimation with a smaller error because of high linear correlation
29 with temperature both in vitro and in vivo. Compared with most previous research
30 which only based on biomaterial in vitro, the in vivo experiment conducted in this
31 paper verified the feasibility of the noninvasive temperature estimation method
32 proposed in practice.

33 **Keywords:** Ultrasound; Noninvasive temperature estimation; Radio frequency
34 ablation; Wavelet transform; Gray-level gradient co-occurrence matrix

36 **Background**

37 Tumor hyperthermia is a therapy that raising the tumor tissue to a certain high
38 temperature by heating to make it inactive and die. It has been widely used in clinical
39 tumor treatment. Hyperthermia methods mainly include microwave ablation,
40 high-energy ultrasound (HIFU), radio frequency ablation (RFA), etc. Among them,
41 RFA has become one of the most common heating methods which using thermal
42 effect of radio frequency current to form a high temperature thermal coagulation area
43 to kill the tumor cells by releasing the radio frequency alternating current^{[1][2]}.

44 For tumor tissue, low pH environment caused by long-term energy consumption and
45 lack of basement membrane lead to its poor heat resistance. When the temperature
46 reaches 40 °C ~ 43 °C, DNA damage and cell death will occur; when the temperature
47 exceeds 45°C to 50°C, the protein in normal tissue cells will be denatured and the
48 tissue will be dehydrated^[3]. Therefore, it is particularly important to make sure that
49 the temperature is controlled within a suitable range in hyperthermia so that it can kill
50 tumor cells effectively and avoid causing damage to surrounding normal tissues. In
51 recent years, many noninvasive temperature estimation methods related to tumor
52 hyperthermia have been proposed, including magnetic resonance imaging(MRI)^{[4][5]},
53 electrical impedance tomography(EIT)^[6], ultrasound, etc., among which ultrasound
54 has become one of the most popular research directions in this field due to its various
55 advantages of simple operation, safety, high resolution and real-time data processing.
56 In the field of noninvasive temperature estimation based on ultrasound, the area of
57 image-guided is always the focus of the research. In 2002, Hou studied the correlation
58 between gray value and temperature during HIFU with pig liver in vitro, and came up
59 with the conclusion that gray value of the B-ultrasound image has a certain nonlinear
60 relationship with temperature^[7]. In 2010, Yang used pig liver in vitro to study the
61 correlation between B-ultrasound tissue texture features and temperature in
62 microwave ablation experiment, and verified that changes in image features can
63 reflect the temperature of tissue^[8]. In 2015, Li Yong processed the B-ultrasound
64 images obtained after HIFU of pork with method based on gray probability
65 distribution-cross entropy, and demonstrated that the cross-entropy of the data is

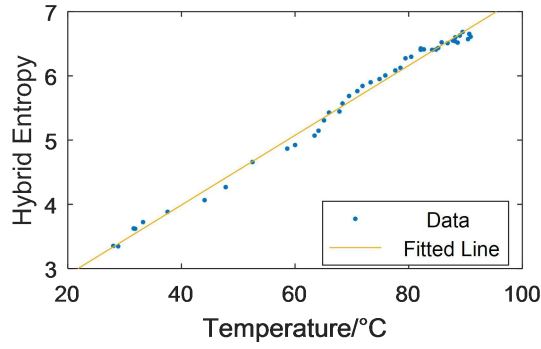
66 approximately linear with the temperature ^[9]. In 2018, Guo proposed a BEMD-RF
67 method based on machine learning, which provides a new idea for noninvasive
68 temperature estimation^[10]. Most of the previous research conclusions are based on in
69 vitro experiments. Therefore, in order to make the experimental results more universal,
70 this paper took animal tissue both in vitro and in vivo as experimental materials, using
71 wavelet transform and gray-level gradient co-occurrence matrix as image process
72 methods to explore the linear correlation between image texture features and
73 temperature under different conditions.

74

75 **Results**

76 After performing wavelet transform on each set of subtraction ultrasound images, the
77 texture feature hybrid entropy and energy of the gray-level gradient co-occurrence
78 matrix were extracted and linearly fitted with temperature data by using the least
79 square method.

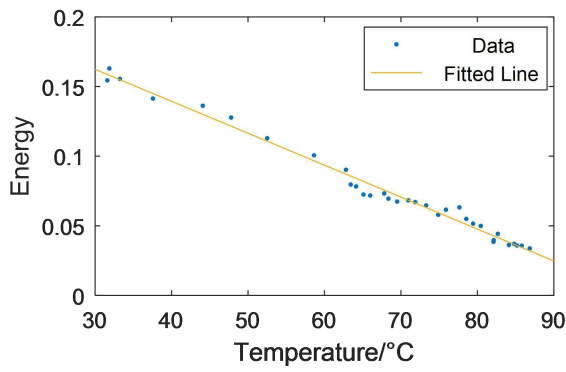
80 The correlation between texture features and temperature in vitro experiment are
81 shown in Fig.1, and multiple sets of data have high consistency. The linear correlation
82 coefficient of hybrid entropy reaches 0.979 ± 0.028 , and the linear correlation
83 coefficient of energy reaches -0.935 ± 0.037 .



84

85

(a) Correlation between hybrid entropy and temperature



86

87

(b) Correlation between energy and temperature

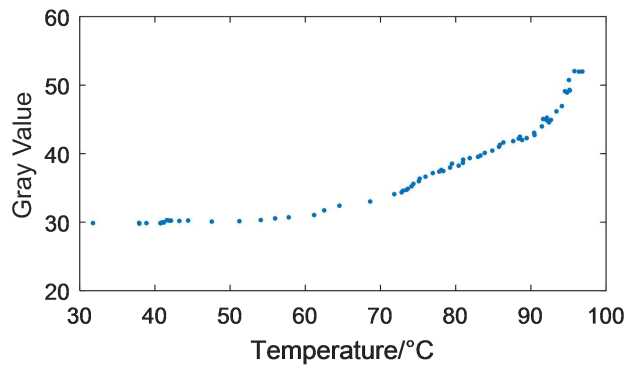
88

Fig.1 Correlation between texture features and temperature in vitro experiment

89 In addition, gray value of the ultrasound image from in vitro experiment was also

90 extracted for comparative analysis, and the correlation with temperature is shown in

91 Fig.2.



92

93

Fig.2 Correlation between gray value and temperature in vitro experiment

94 By comparing Fig.1 and Fig.2, it can be seen that under in vitro condition, gray value

95 increases slowly in low temperature section but rapidly in high temperature section,
 96 which cannot be evaluated by a linear model and lead to a larger estimation error.
 97 However, hybrid entropy extracted from processed image increases linearly with
 98 temperature, while energy decreases linearly with temperature. In the entire
 99 temperature range, they have more obvious linear correlation with temperature.
 100 Compared with traditional gray value method, it can achieve a larger range of
 101 accurate temperature estimation.
 102 The temperature value of the region during ablation was calculated using the
 103 correlation model of hybrid entropy and temperature obtained before, and the
 104 pseudo-color images of temperature distribution of the region at different stages of
 105 ablation are shown in Fig.3.

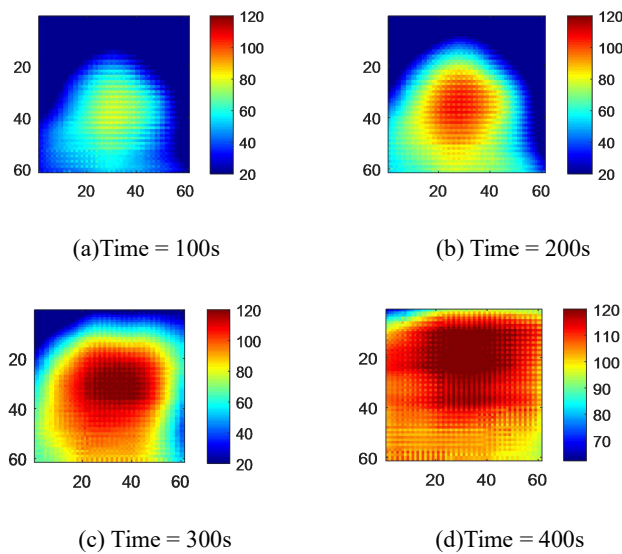
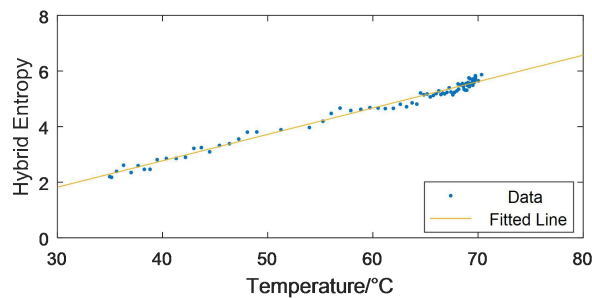


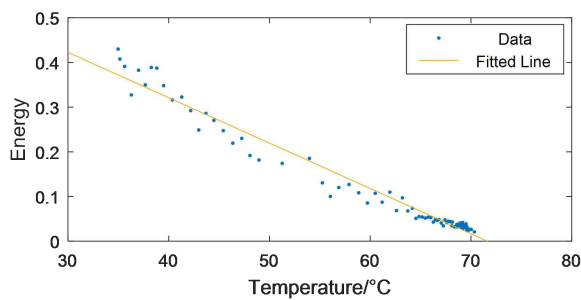
Fig. 3 Pseudo-color image of temperature distribution

111 It can be seen from Fig.3 that the estimated temperature decreases from the radio
 112 frequency probe to the surroundings. As the ablation heating process going on,
 113 temperature in the calculated area gradually increases, which is consistent with the

114 actual temperature measured by the temperature probe. Therefore, it can be said that
115 the linear regression model obtained can complete the temperature estimation work in
116 the whole stage of radio frequency ablation in vitro.
117 Hybrid entropy and energy extracted from in vivo experiment based on wavelet
118 transform and the gray-level gradient co-occurrence matrix change linearly with
119 temperature, which is similar to the rule under in vitro conditions. The correlation is
120 shown in Fig.4. The linear correlation coefficient of hybrid entropy reaches
121 0.932 ± 0.056 , and the linear correlation coefficient of energy reaches -0.915 ± 0.034 .



123 (a) Correlation between hybrid entropy and temperature

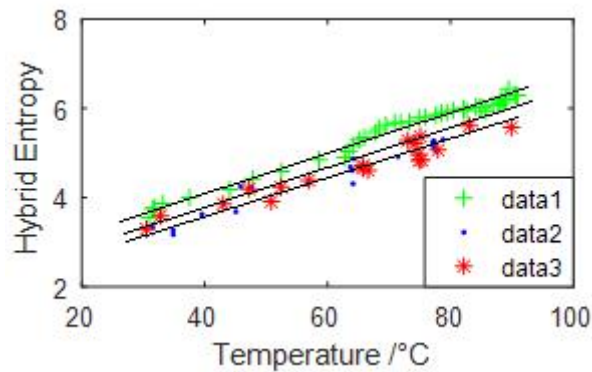


125 (b) Correlation between energy and temperature

126 Fig.4 Correlation between features and temperature from in vitro experiment

127 By comparing the data under two different conditions, it can be seen that the image
128 texture features hybrid entropy and energy have a strong linear correlation with
129 temperature both in vivo and in vitro, which verifies that the image processing method

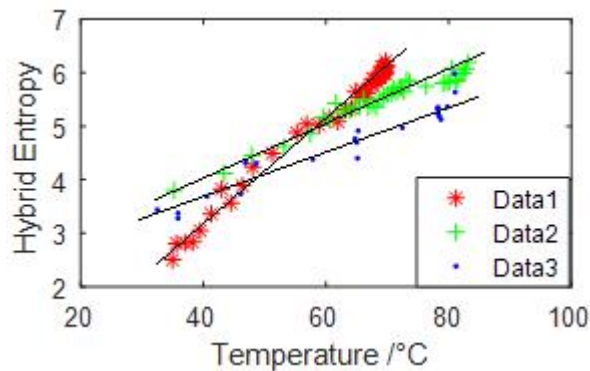
130 proposed has certain feasibility in practice. In addition, the linear model slopes
131 obtained from multiple sets of experimental data under in vitro condition have strong
132 consistency as shown in Fig.5, while those under in vivo condition have certain
133 individual difference as shown in Fig.6.



134

135

Fig.5 Correlation between hybrid entropy and temperature in multiple sets of data in vitro



136

137

Fig.6 Correlation between hybrid entropy and temperature in multiple sets of data in vitro

138 It is speculated that the factors of slope difference between groups in vivo mainly
139 include the following two points: (1) Difference in the ablation speed. Although the
140 measured temperature was constantly rising in all groups, the duration of ablation at
141 the same temperature was not the same. Therefore, image texture feature
142 corresponding to the same temperature in different groups could be very different
143 which had a certain impact on the linear relationship of feature and temperature in

144 different groups in vivo. (2) Difference in biological materials. The biological tissue
145 characteristics of different rabbits for experiment were varied widely, so the
146 individual differences could be one of the most important factors which affect the
147 consistency of multiple sets of data.

148

149 **Conclusion**

150 This paper proposed a noninvasive temperature estimation method based on B-mode
151 ultrasound image using wavelet transform and gray-level gradient co-occurrence
152 matrix. It explored the relationship between texture features of ultrasound image and
153 temperature both in vitro and in vivo. The radio frequency ablation experiments were
154 performed on two kinds of biological material (pig kidney in vitro and rabbit kidney in
155 vivo), during which the ultrasound image and temperature data were collected. After
156 data acquisition, wavelet transform was performed on ultrasound subtraction image to
157 enhance the detailed texture, and features of the gray gradient-level co-occurrence
158 matrix that have a high correlation with temperature were extracted from processed
159 image.

160 It is shown that under the two different experimental conditions, hybrid entropy and
161 energy extracted with this method have an obvious linear relationship with
162 temperature. The slopes of linear regression model obtained in vitro are relatively
163 consistent, while those under in vivo condition have certain differences affected by
164 ablation rate and the individual differences in tissue characteristics of biomaterials.
165 The result under in vivo condition verifies the feasibility of the noninvasive

166 temperature estimation method proposed in practice. However, the process of in vivo
167 experiment still has some shortcomings.

168 Although the rabbits in experiment were anesthetized, it was impossible to avoid the
169 influence of breathing and other tiny movements on the positioning of the area of
170 interest. In this paper, the manual positioning method we used is more
171 time-consuming, so some automatic positioning methods will be designed to achieve
172 high efficiency and accuracy in segmentation in future work . In addition, although
173 the models obtained from multiple groups of in vivo experiments have high linear
174 correlation, there is still some difference in slope. Therefore, how to eliminate the
175 differences and establish a general prediction model is still the focus of exploration in
176 the future research.

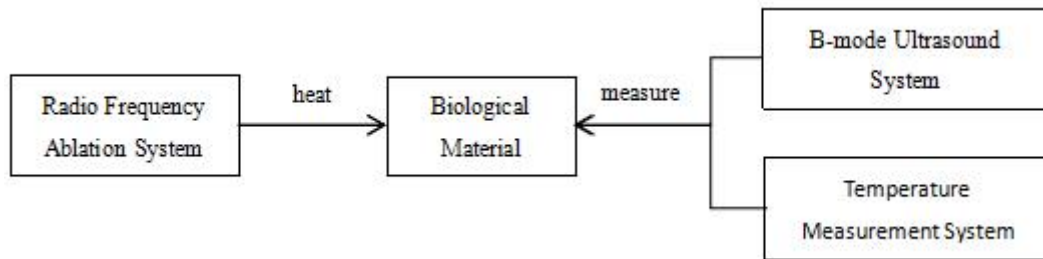
177

178 **Methods**

179 **Experimental system**

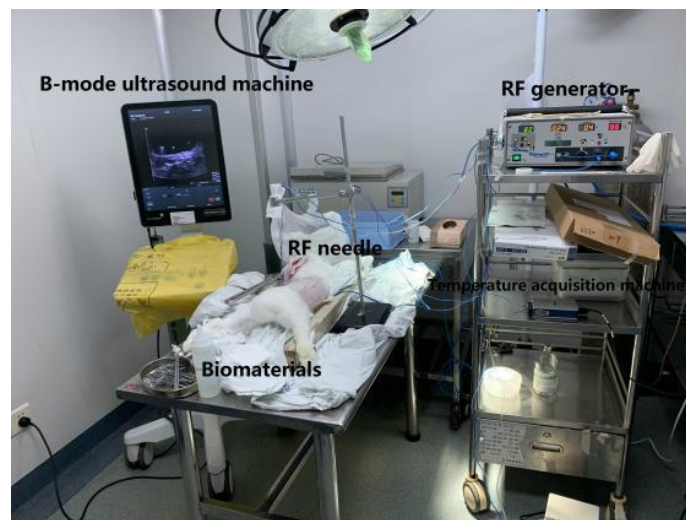
180 The experimental system consists of radio frequency ablation system, temperature
181 measurement system, B-mode ultrasound machine and biological materials, as shown
182 in Fig.7. The experimental platform is shown in Fig.8. The radio frequency ablation
183 system Cool-tip from Valleylab is mainly composed of radio frequency generator with
184 an adjustable power in the range of 0W~200W, a radio frequency electrode and
185 condensing circulatory system. The radio frequency ablation in experiment is guided
186 by B-ultrasound machine Flex Focus 800 from BK medical company with convex
187 array 8233 ultrasonic probe. The temperature measurement system is based on

188 NI9213 thermocouple temperature measurement module with a conversion time of
189 55ms and a channel sampling rate of 1 sample/s, the temperature data which collected
190 can be displayed and stored in real time on the computer.



191
192

Fig.7 Experiment scheme



193
194

Fig.8 Experiment platform

195 As for experimental materials, pig kidney tissue and rabbit kidney tissue are both
196 similar to human kidney tissue in composition. For in vitro experiment, due to larger
197 size and contact area with the thermal ablation plate which were conducive to the
198 experiment, pig kidney was chosen as experimental material. For in vivo experiment,
199 rabbit kidney in vivo was used as the biological material because breathing and other
200 motions of rabbit under anesthesia were smaller so that there would be fewer factors
201 unrelated to the experiment.

202 **Experimental method**

203 The experiment was conducted according to the following two steps. (1) Pretreatment
204 of biological materials: The rabbit was anesthetized with its kidney exposed as
205 ablation experiment material by surgery and abdomen dehaired to ensure its good
206 contact with the electrode plate. The pig kidney in vitro was placed horizontally on
207 the electrode plate to ensure good contact with the electrode plate. After placing the
208 biological materials, the radio frequency ablation probe and temperature probe should
209 be inserted vertically into the kidney with a depth of about 1 cm so that the two probe
210 tips would be on the same horizontal line. After the probes were placed, B-ultrasound
211 probe should be placed close to the surface of the kidney and perpendicular to the the
212 other two probes and ensured that its center height would be the same as the height of
213 the other two probe tip. (2) Radio frequency ablation and data acquisition: Based on
214 previous experience ^[11], the duration of ablation was set to 8min, and the ablation
215 power was adjusted manually during the experiment to make sure the temperature
216 change steady. Radio frequency ablation system, ultrasound image system and
217 temperature measurement system were turned on at the same time, and 2 minutes after
218 ablation finished, image recording of the B-mode ultrasound machine and temperature
219 measurement system were stopped simultaneously.

220 **Image preprocessing**

221 The video frame rate of the ultrasound image obtained is 22 frames/s. In order to
222 eliminate random noise and make the sampling frequency of ultrasound image and
223 temperature data the same, we calculated the average value of each pixel of the

224 ultrasound image per second . The ultrasound images before and after the ablation are
225 shown in Fig.9.



226

227 (a) Ultrasound image before ablation experiment (b) Ultrasound image after ablation experiment

228 Fig.9 Ultrasound images before and after the ablation experiment

229 A 40-pixel×40-pixel region centered on temperature probe was intercepted as the
230 region of interest for processing which corresponding to the temperature obtained. In
231 order to avoid the interference of the temperature probe and reduce the error under
232 different conditions, the difference processing of the ultrasound images before and
233 during RFA was performed, and then wavelet transform and texture analysis were
234 performed on the subtraction image obtained.

235 **Wavelet transform**

236 Wavelet transform has the ability of multi-resolution analysis and characterizing local
237 signals in both time and frequency domains. To perform a two-dimensional discrete
238 wavelet transform on an image, Mallat algorithm can be used to achieve a pyramidal
239 structure of image. After the image is decomposed by wavelet, it will produce two
240 parts, low frequency component and high frequency component. The low frequency
241 component reflects the approximate part of the image, and the high frequency

242 component carries the information of the texture details ^[12].

243 Because we pay more attention to the change of ultrasound image during ablation
244 experiment, the detail components of the wavelet decomposition of the subtraction
245 image were used for wavelet reconstruction to highlight the texture details of the
246 ultrasound image, which provided a basis for the next step of using the gray-level
247 gradient co-occurrence matrix to analyze image texture features.

248 **Gray-Level Gradient Co-occurrence Matrix**

249 Gray-Level Gradient Co-occurrence Matrix (GLGCM) is a method for image texture
250 feature analysis, which reflects not only the gray spatial distribution but also edge
251 gradient information. Gray spatial distribution information is the basis of the image
252 composition, and gradient information constitutes the edge of the image. The
253 combination of the two key information can better describe texture characteristics of a
254 image^[13].

255 The operational processes of how to extract the gray-gradient co-occurrence matrix
256 from a image are as follows. $f(i, j)$ is the gray image to be processed, from which we
257 can obtain gradient image $g(i, j)$ by using gradient operator. The gray matrix $F(i, j)$
258 and gradient matrix $G(i, j)$ can be obtained from these images by regularization
259 processing shown in Eq.1 and Eq.2, where L and L_g are number of gray levels of
260 gray image and gradient image respectively, f_{\max} and g_{\max} are the max value of gray
261 image and gradient image respectively.

$$262 \quad F(i, j) = \frac{f(i, j)L}{f_{\max}} + 1 \quad \text{Eq.1}$$

263
$$G(i, j) = \frac{g(i, j)L_g}{g_{\max}} + 1 \quad \text{Eq.2}$$

264 The gray gradient co-occurrence matrix $H(x, y)$ is donated as the number of the
 265 pixels, which gray value is x in $F(i, j)$ and the gradient is y in $G(i, j)$. In order to
 266 simplify the calculation, the gray-level gradient co-occurrence matrix is normalized to
 267 make the sum of every element to be 1, as shown in Eq.3.

268
$$H'(i, j) = \frac{H(i, j)}{\sum_{i=0}^{L-1} \sum_{j=0}^{L_g-1} H(i, j)} \quad \text{Eq.3}$$

269 Based on the normalized gray gradient co-occurrence matrix, 15 second-order feature
 270 parameters can usually be used to describe the texture characteristics of the image,
 271 including small gradient dominance, large gradient dominance, gray mean, gradient
 272 mean, gray entropy, gradient entropy, hybrid entropy, gray asymmetry, gradient
 273 asymmetry, energy, gray standard deviation, gradient standard deviation, correlation,
 274 inertia and inverse difference moment. Based on the research characteristics, hybrid
 275 entropy and energy were selected as the characteristics to estimate temperature, as
 276 shown in Eq.4 and Eq.5.

277 Hybrid entropy:

278
$$T_1 = -\sum_{i=0}^{L-1} \sum_{j=0}^{L_g-1} H'(i, j) \log_2 H'(i, j) \quad \text{Eq.4}$$

279 Energy:

280
$$T_2 = \sum_{i=0}^{L-1} \sum_{j=0}^{L_g-1} H'^2(i, j) \quad \text{Eq.5}$$

281

282 **References**

283 [1] Shultz Kim, Stang Pascal, Kerr Adam, Pauly John, Scott Greig. RF field visualization of RF
284 ablation at the Larmor frequency.[J]. IEEE transactions on medical imaging, 2012, 31(4).

285 [2] Giulio Di Candio MD, Francesco Porcelli MD, Alessandro Campatelli MD, et al.
286 High-Intensity Focused Ultrasonography and Radiofrequency Ablation of Renal Cell Carcinoma
287 Arisen in Transplanted Kidneys: Single-Center Experience With Long-Term Follow-Up and
288 Review of Literature. 2019, 38(9):2507-2513.

289 [3] Hildebrandt B, Wust P, Ahlers O, et al. The cellular and molecular basis of hyperthermia[J]. Crit
290 Rev Oncol Hema. tol, 2002, 43 (1) :33.56.

291 [4] Hue Yik-Kiong, Guimaraes Alexander R, Cohen Ouri, Nevo Erez, Roth Abraham, Ackerman
292 Jerome L. Magnetic Resonance Mediated Radiofrequency Ablation.[J]. IEEE transactions on
293 medical imaging, 2018, 37(2).

294 [5] Jenista, Branca, Warren. Absolute temperature imaging using intermolecular multiple quantum
295 MRI. International Journal of Hyperthermia, 2010, 26(7):725-734.

296 [6] H. Woo, Y. Kim, A. Guy. Feasibility Study of Monitoring Temperature Rise in Muscle Phantoms
297 by the Electrical Impedance Tomography System During Hyperthermia Treatment[J]. Journal of
298 Microwave Power and Electromagnetic Energy, 2016, 25(4).

299 [7] Hou Z X, et al. A new experimental study on noninvasive thermometry in HIFU[J]. Journal of
300 Harbin Institute of Technology, 2002(03):259-262.

301 [8] Yang Chunlan, Zhu Hao, Wu Shuicai, et al. Correlations between B-mode ultrasonic image
302 texture features and tissue temperature in microwave ablation.. 2010, 29(12):1787-99.

303 [9] LI Yong, DING Yajun, QIAN Shengyou, et al. Noninvasive temperature estimation method
304 based on gray probability distribution-cross entropy[J]. Journal of Electronic Measurement and

305 Instrumentation,2015,29(02):247-251.

306 [10] GUO Yan, DING Yajun, QIAN Shengyou, CHEN Xing. Noninvasive Temperature
307 Measurement Based on BEMD and Random Forest Algorithm in High Intensity Focus Ultrasound
308 Therapy[J]. Journal of Test and Measurement of Technology,2018,32(06):487-492.

309 [11] CUI Mengyao, YING Xiaoting, ZHAO Xingqun, YAO Linfang. Correlation between renal
310 ultrasound image features and temperature during radio frequency ablation. Chinese Journal of
311 Medical Physics, 2020, 37(9): 1164-1168.

312 [12] Kim Yong Sun,Ra Jong Beom. Speckle Noise Reduction and Edge Enhancement in
313 Ultrasound Images Based on Wavelet Transform[J]. Journal of Biomedical Engineering
314 Research,2008,29(2).

315 [13] Lam SW-C. Texture feature extraction using gray level gradient based co-occurrence matrices.
316 1996 IEEE International Conference on Systems, Man and Cybernetics Information Intelligence
317 and Systems (Cat No96CH35929). 1996;1:267.

318

319 **Declaration**

320 **Ethics approval and consent to participate**

321 The experiment was approved by the ethics committee of Nanjing Drum Tower
322 Hospital, the Affiliated Hospital of Nanjing University Medical School, Nanjing,
323 China. Animals were managed according to the guidelines of the American
324 Physiological Society.

325 **Consent for publication**

326 Not applicable.

327 **Availability of data and material**

328 The datasets during and/or analysed during the current study available from the
329 corresponding author on reasonable request.

330 **Competing interests**

331 The authors declare that they have no competing interests.

332 **Funding**

333 None declared.

334 **Author information**

335 **Affiliations**

336 School of Biological Science and Medical Engineering, Southeast University, Nanjing,
337 China

338 Ming Chen & Xingqun Zhao

339 Department of Urology, Nanjing Drum Tower Hospital, the Affiliated Hospital of
340 Nanjing University Medical School, Nanjing, China

341 Linfang Yao

342 **Authors' contributions**

343 MC contributed to data collection, processing, analysis and manuscript drafting. LY
344 and MC contributed to design and operation of the experiment. XZ and LY
345 contributed to the manuscript revision. All authors approve the final version of the
346 manuscript.

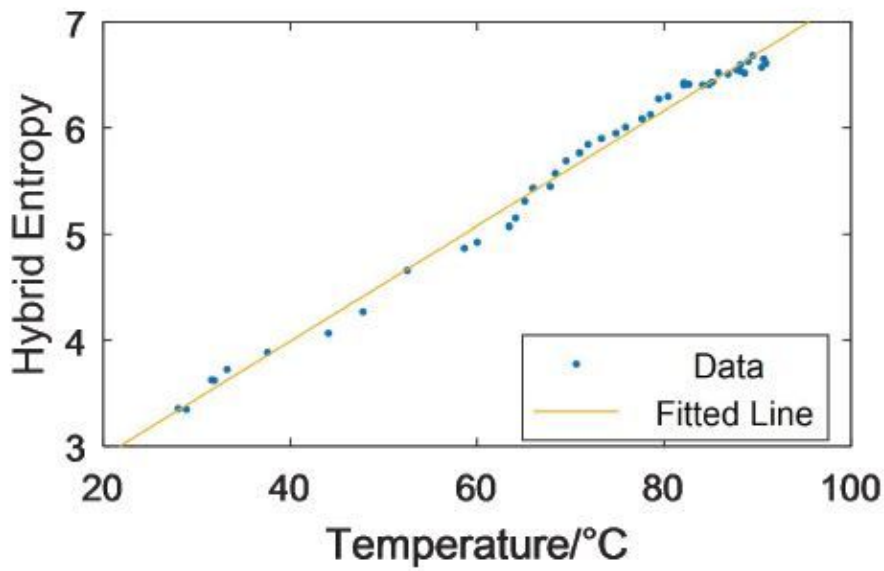
347 **Corresponding author**

348 Correspondence to Xingqun Zhao & Linfang Yao.

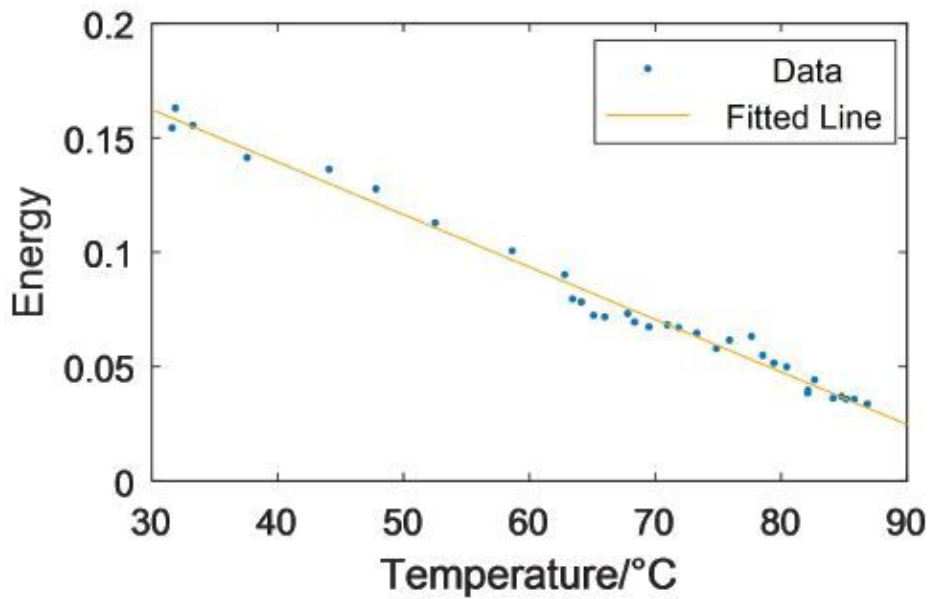
349 **Acknowledgements**

350 Not applicable.

Figures



(a) Correlation between hybrid entropy and temperature



(b) Correlation between energy and temperature

Figure 1

Correlation between texture features and temperature in vitro experiment

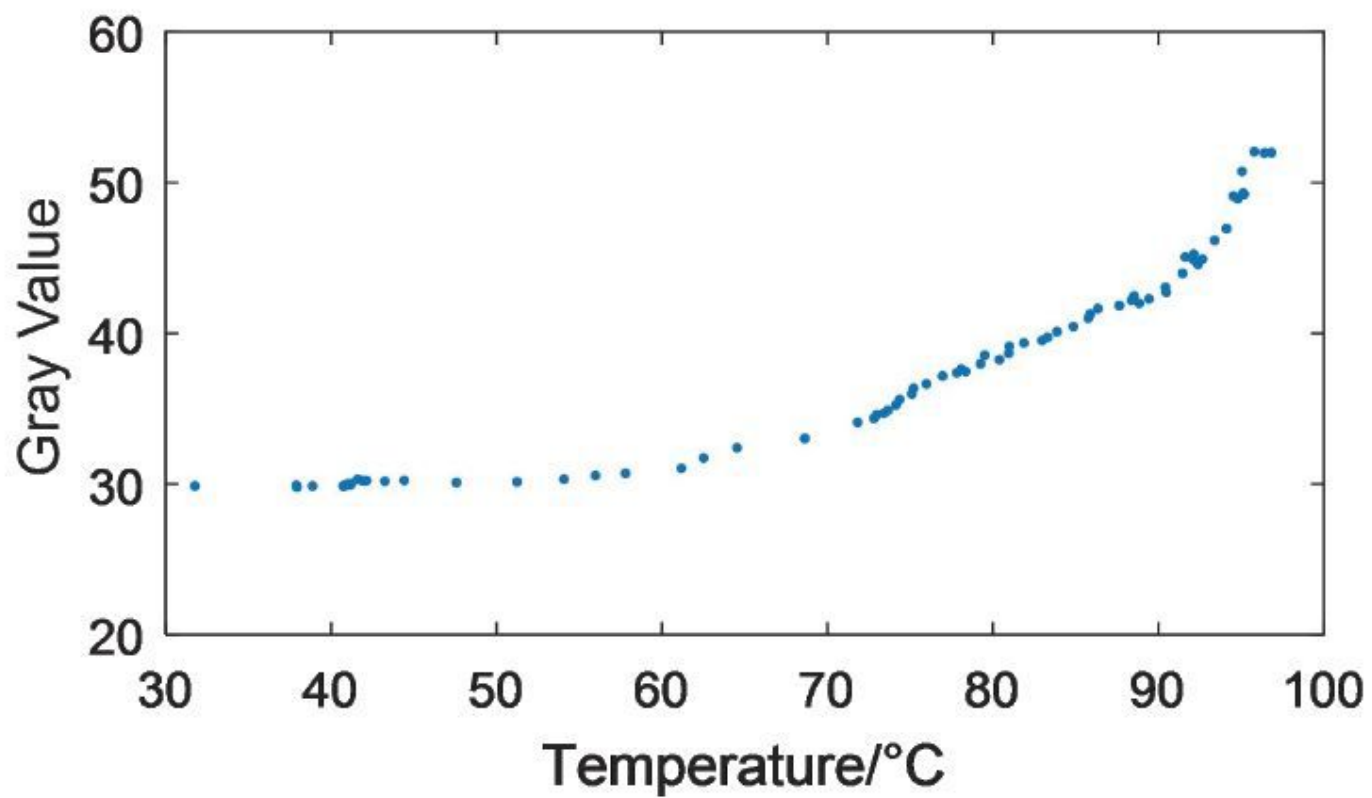
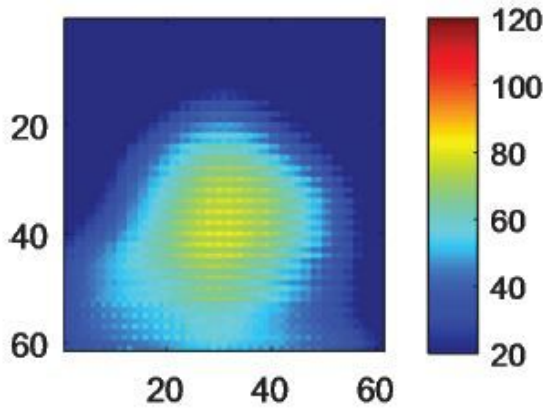
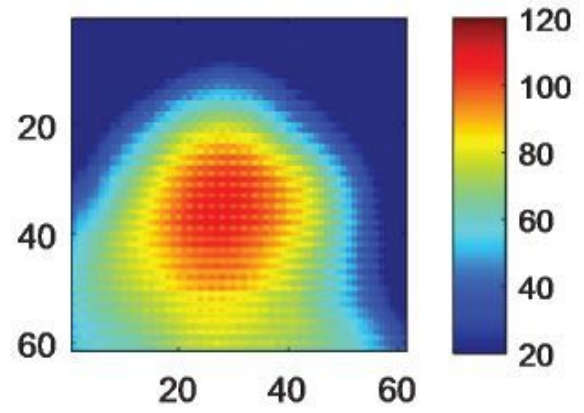


Figure 2

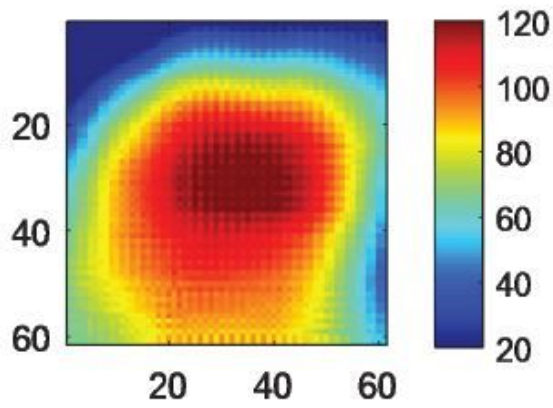
Correlation between gray value and temperature in vitro experiment



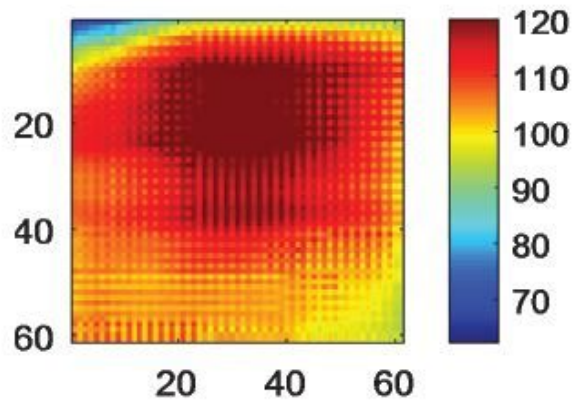
(a) Time = 100s



(b) Time = 200s



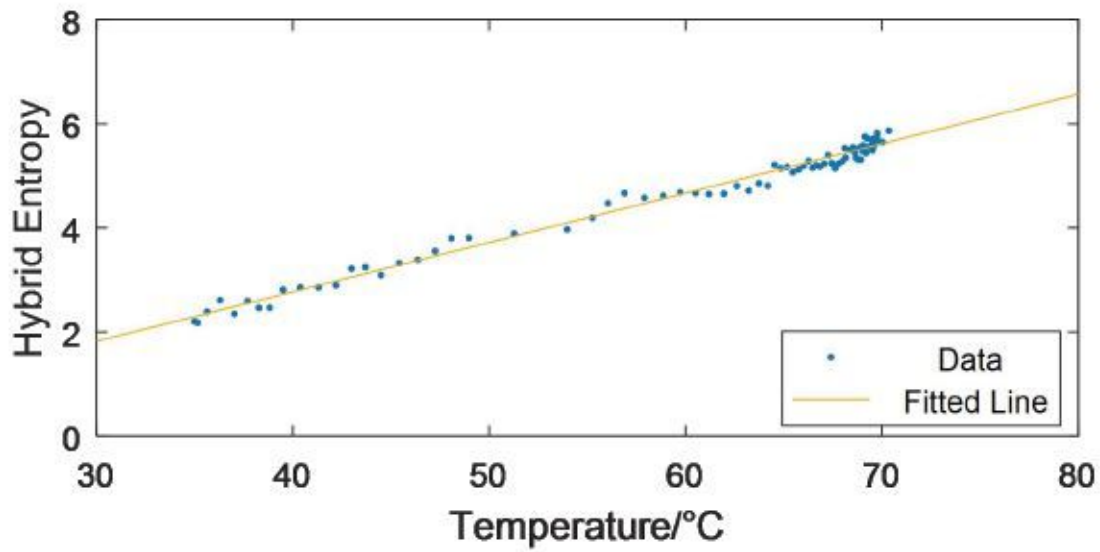
(c) Time = 300s



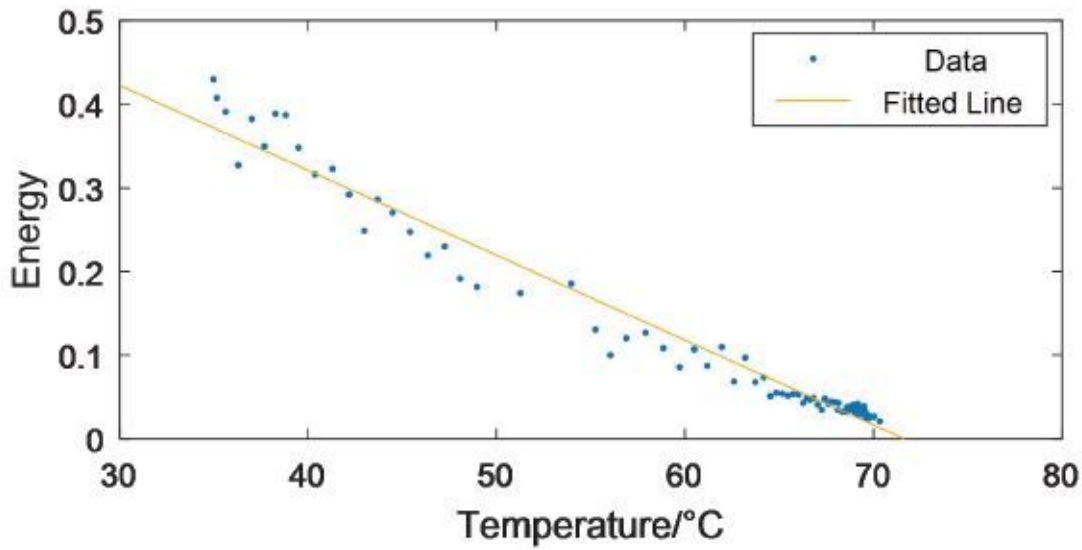
(d) Time = 400s

Figure 3

Pseudo-color image of temperature distribution



(a) Correlation between hybrid entropy and temperature



(b) Correlation between energy and temperature

Figure 4

Correlation between features and temperature from in vitro experiment

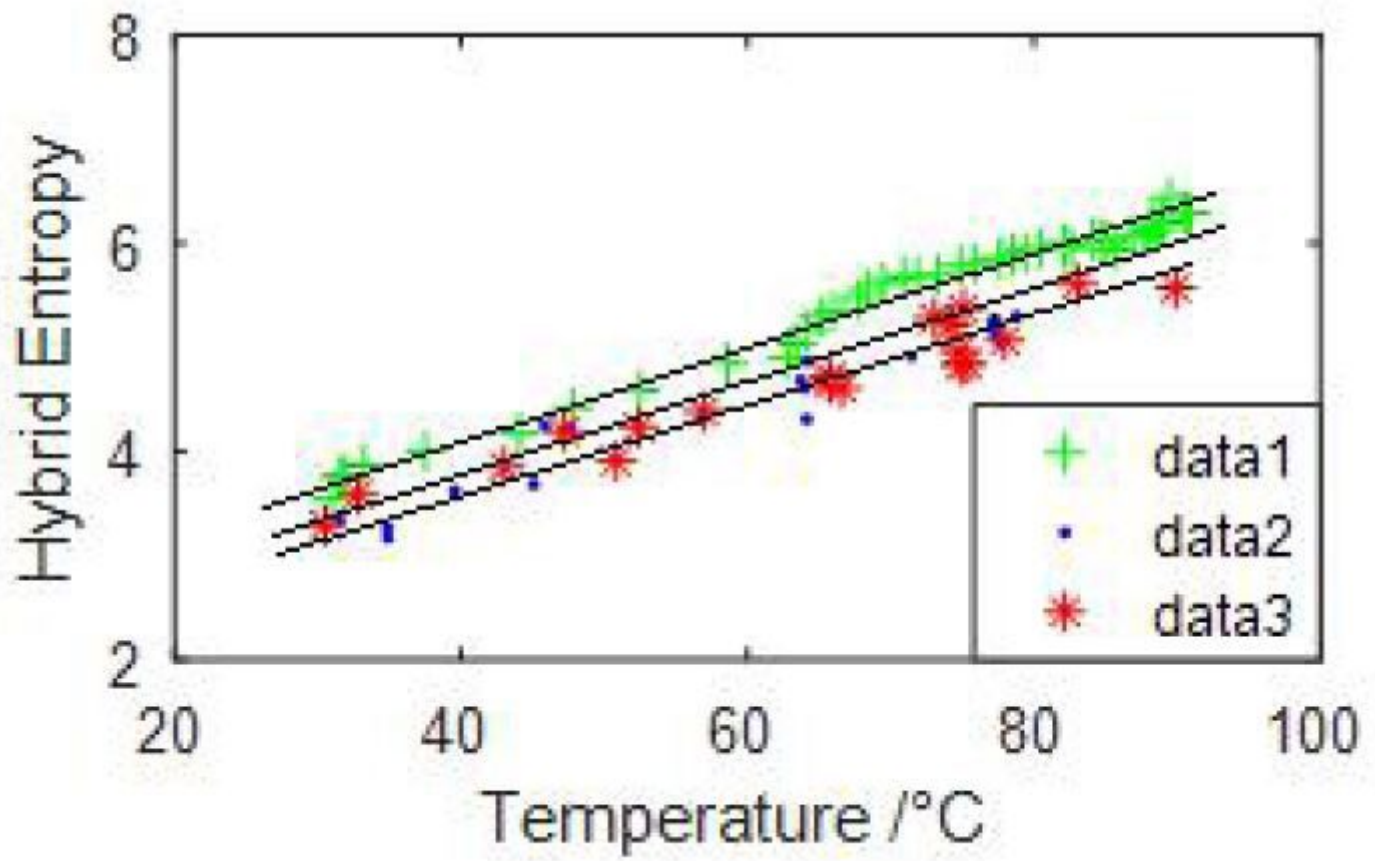


Figure 5

Correlation between hybrid entropy and temperature in multiple sets of data in vitro

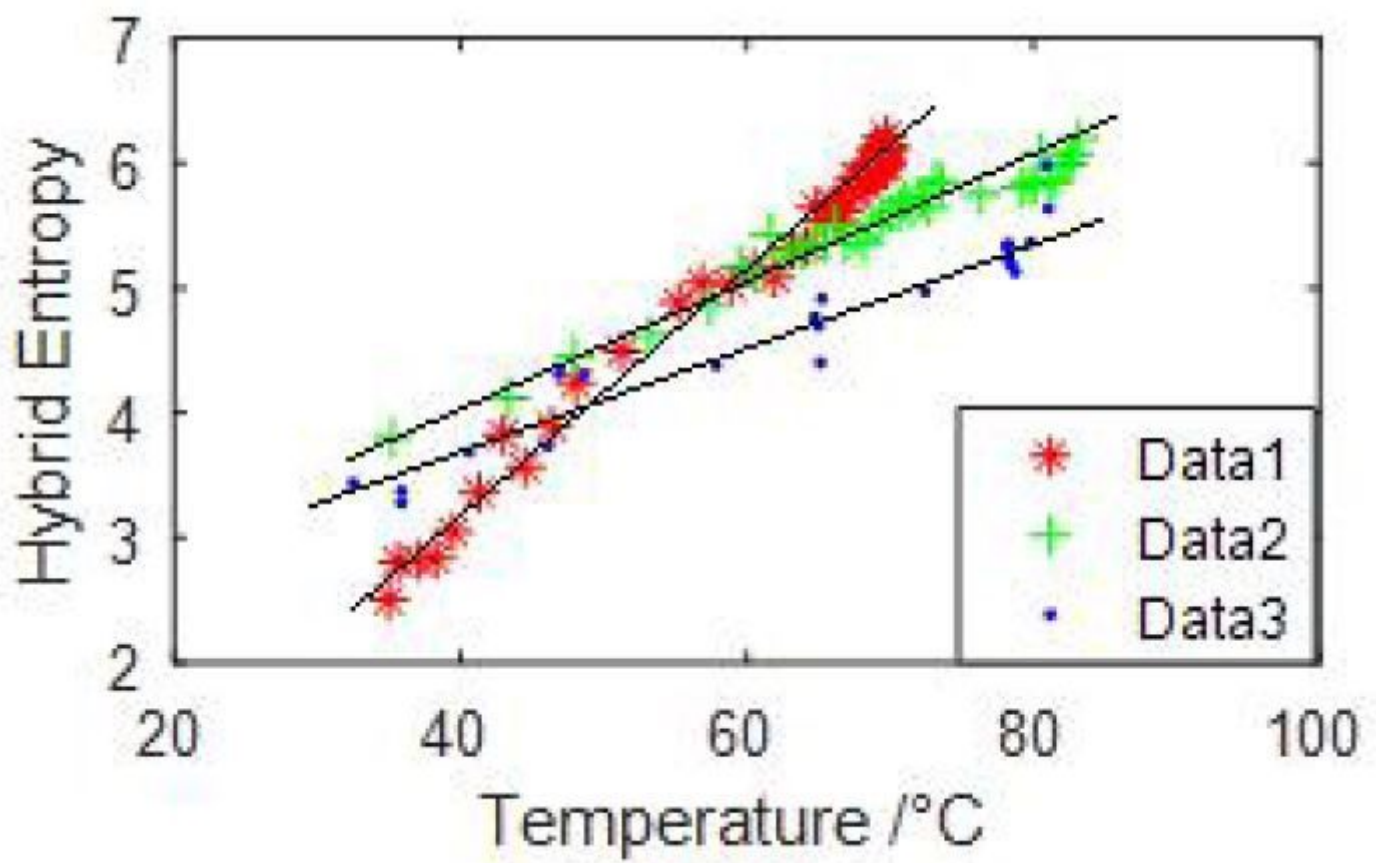


Figure 6

Correlation between hybrid entropy and temperature in multiple sets of data in vitro

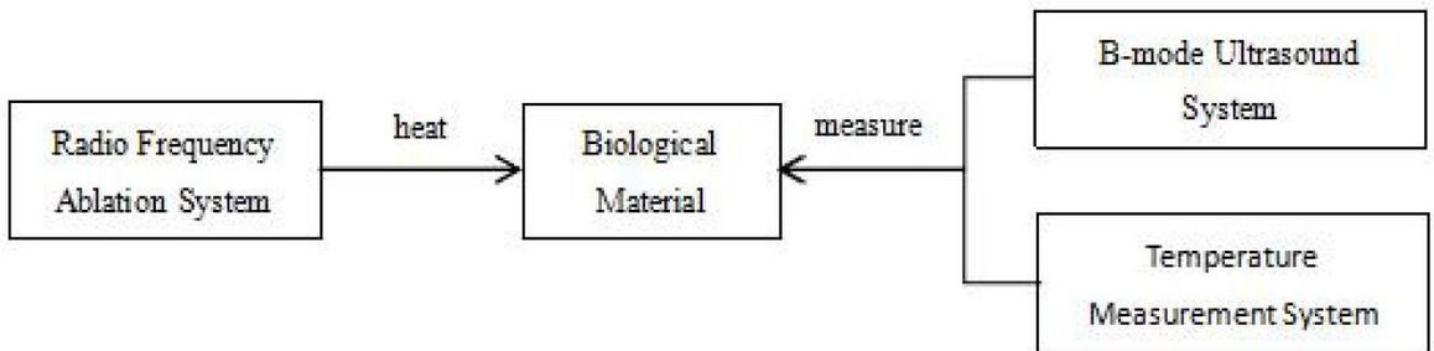


Figure 7

Experiment scheme

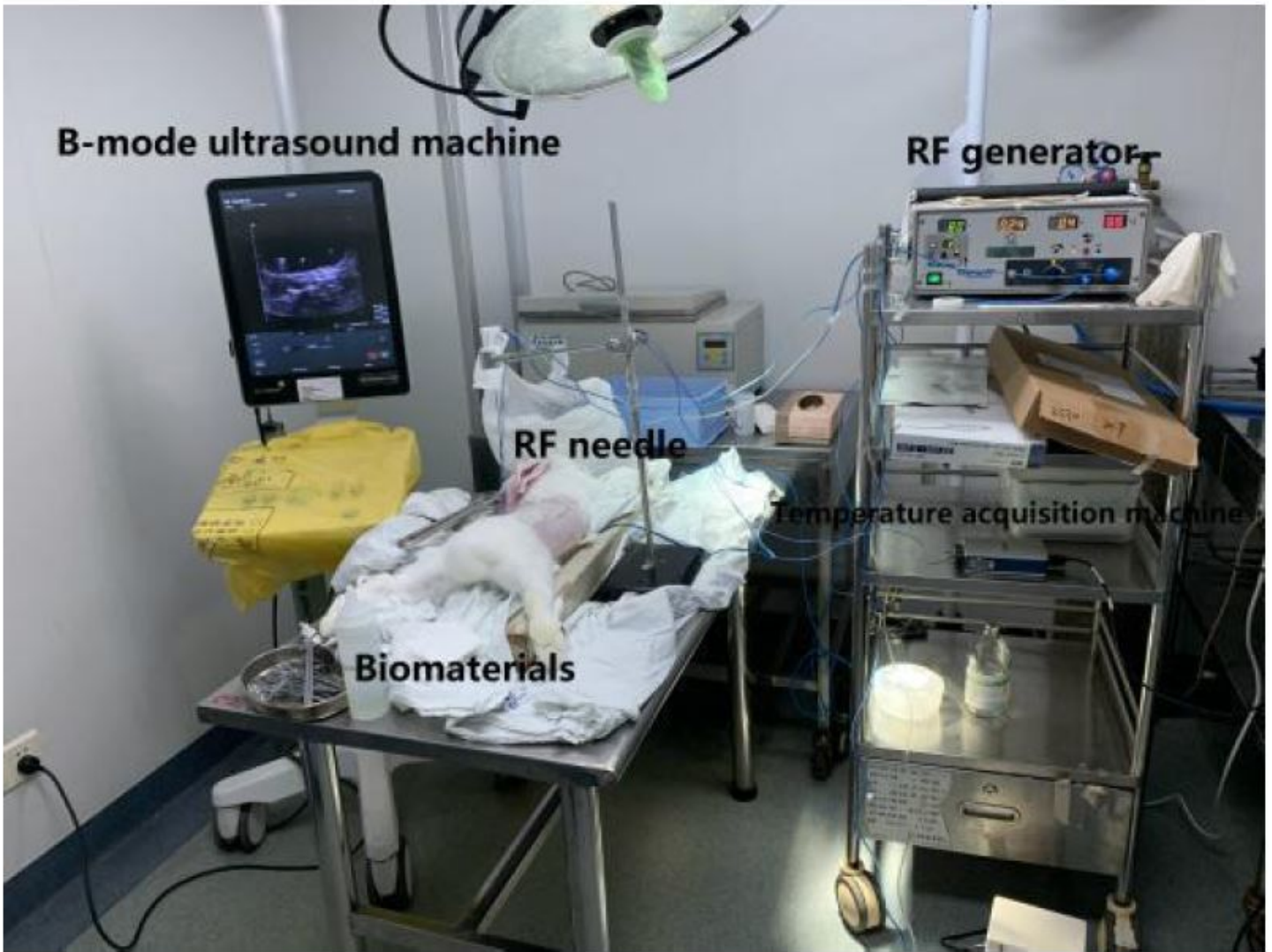
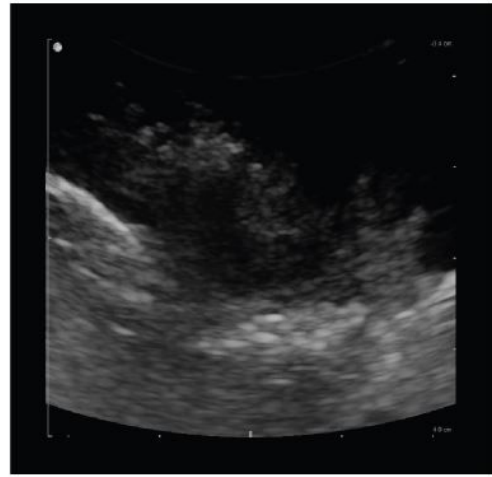
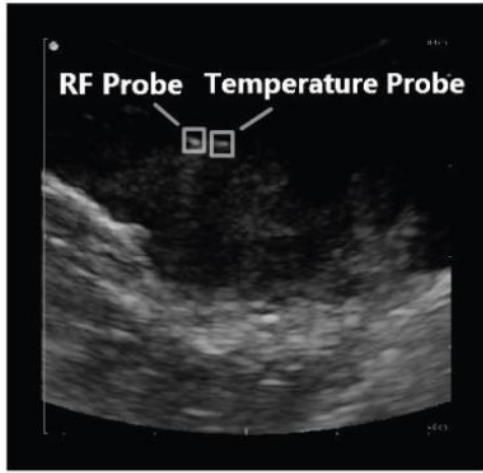


Figure 8

Experiment platform



(a) Ultrasound image before ablation experiment

(b) Ultrasound image after ablation experiment

Figure 9

Ultrasound images before and after the ablation experiment. (a) Ultrasound image before ablation experiment (b) Ultrasound image after ablation experiment